Antisense oligonucleotide-mediated redirection of Igf1 alternative polyadenylation

Yavas, A.; Putten, M. van; Ariyurek, Y.; Aartsma-Rus, A.

Neuromuscular Disorders 51 (2025) 105394

Contents lists available at ScienceDirect

Neuromuscular Disorders

journal homepage: www.elsevier.com/locate/nmd

Antisense oligonucleotide-mediated redirection of *Igf1* alternative polyadenylation

Alper Yavas *, Maaike van Putten, Yavuz Ariyurek, Annemieke Aartsma-Rus

Department of Human Genetics, Leiden University Medical Center, Leiden, the Netherlands

ARTICLE INFO

Keywords:
Muscle wasting disorders
Insulin-like growth factor-1
Downhill treadmill exercise
Alternative polyadenylation
Antisense oligonucleotides

ABSTRACT

Insulin-like growth factor-1 (IGF-1) has become an interesting potential therapeutic target for muscle wasting disorders, since it is known to modulate muscle growth and function. Alternative polyadenylation (APA) *Igf1* gives rise to 3′UTR isoforms with different stability and translation efficiency due to their length and context-dependent miRNA binding sites. *Igf1* transcripts with a shorter 3′UTRs are thought to be more stable and efficient during protein translation. Therefore, modulating the *Igf1* polyadenylation site usage would be a potential approach to increase IGF-1 protein expression. In this study, we first investigated the *Igf1* 3′UTR isoforms in exercised *mdx* and WT mice by full-length isoform sequencing. We then redirected the APA of *Igf1* from the distal to the proximal/middle polyadenylation sites to enhance the IGF-1 protein expression in mouse C2C12 myoblasts. Upon exercise, APA of *Igf1* was redirected towards the proximal polyadenylation site in the WT mice only ($P < 0.05$). Transfection of C2C12 cells with this AON resulted in redirection of the APA towards the proximal site and increased IGF-1 expression/AKT phosphorylation levels. Strong enrichment was found for genes involved in sarcomere organization, muscle cell development and calcium homeostasis. Our study reports the effect of downhill running exercise on the *Igf1* 3′UTRs in *mdx* and WT mice and provides an *in vitro* proof of principle for redirecting the *Igf1* poly(A) site usage as a strategy to increase protein expression without modifying the coding region of the gene, not only for IGF-1 but also for other targets with therapeutic potential in different conditions.

1. Introduction

Duchenne muscular dystrophy (DMD) is an X-linked neuromuscular disorder, affecting 1 in 5000 boys, caused by mutations that disrupt dystrophin expression [1]. Dystrophin plays a critical role in stabilizing muscle fibers by linking the actin cytoskeleton to the extracellular matrix. Without dystrophin, muscle fibers become fragile and prone to contraction-induced damage, triggering cycles of degeneration, regeneration, and inflammation [2]. Over time, impaired muscle repair leads to the replacement of muscle fibers with fibrotic and adipose tissue, worsening disease progression [3]. While therapies targeting the primary gene defect exist, challenges such as immune responses, inefficient delivery, and mutation specificity limit their effectiveness and applicability [4]. Therefore, alternative strategies that enhance muscle quality and function by addressing secondary pathological mechanisms have gained increasing interest.

Insulin-like growth factor-1 (IGF-1) is a key regulator of muscle growth, regeneration, and repair, making it a promising therapeutic target for DMD [5]. Various strategies have been explored to increase IGF-1 signaling, including systemic recombinant IGF-1 administration. However, this approach is limited by the presence of IGF-binding proteins, which restrict the bioavailability of IGF-1 in muscle, and by the complexity of IGF-1 isoforms and posttranslational modifications [6–8].

Alternative polyadenylation (APA) mediates the dynamic usage of the 3′UTR and plays a significant role in post-transcriptional regulation under different pathological and physiological conditions [9]. In *Igf1*, there are three polyadenylation sites located in the last exon (Fig. 1). The usage of the canonical distal polyadenylation site forms a 6.7 kb long UTR, while 200 nt and 1.2 kb long 3′UTRs are produced when the proximal and the middle polyadenylation sites are utilized, respectively [10]. APA contributes to *Igf1* transcript diversity, influencing mRNA stability, localization, and translation efficiency. The use of the long 3′UTR in *Igf1* is often associated with cell differentiation, but these transcripts tend to be less stable due to the presence of AU-rich elements, miRNA suppression, and RNA-binding proteins [10–12]. Shifting polyadenylation site usage from the distal to proximal site could enhance

* Corresponding author at: Dept of Human Genetics, Leiden University Medical Center, Albinusdreef 2, 2333 ZA, Leiden, The Netherlands.
E-mail address: a.yavas@lumc.nl (A. Yavas).

https://doi.org/10.1016/j.nmd.2025.105394
Received 19 December 2024; Received in revised form 23 April 2025; Accepted 22 May 2025
Available online 24 May 2025

IGF-1 expression, thereby improving muscle regeneration and function.

In this study, we investigate *Igf1* 3′UTR patterns in dystrophic and exercised conditions and evaluate the potential of antisense oligonucleotide (AON)-mediated APA redirection to enhance IGF-1 expression. We show that *mdx* mice (a DMD mouse model lacking dystrophin) tend to express shorter *Igf1* 3′UTR compared to wildtype (WT) mice in resting state and that exercise does not change the *Igf1* 3′UTR pattern in *mdx* mice, while creating a significant shift towards the proximal polyadenylation site in WT mice. Furthermore, we demonstrate that 2′-O-methyl phosphorothioate AONs effectively modulate APA in C2C12 muscle cells, leading to increased IGF-1 protein levels and enhanced downstream signaling. Our 3′RNA-seq analysis further reveals differentially expressed genes involved in myogenesis and calcium homeostasis, highlighting APA redirection as a promising therapeutic strategy for DMD and other muscle-related disorders.

2. Materials and methods

2.1. Downhill treadmill running of mdx and WT mice

Male *mdx* (C57BL/10ScSn-Dmd^{mdx}/J) and WT (C57BL/10ScSnJ) mice were bred at the animal facility of the Leiden University Medical Center. Mice were housed in individually ventilated cages, at 20.5 °C with 12-hour dark/light cycles. They had *ad libitum* access to standard RM3 chow (SDS, Essex, United Kingdom) and water. All experiments were approved by and performed following the guidelines of the Animal Experiment Committee of the Leiden University Medical Center (PE.17.246.039). Care was taken to limit the burden and distress for the animals as much as possible.

For the downhill treadmill running exercise, 9 weeks old *mdx* and WT mice ($n = 9$) were acclimatized for 2 min on the stationery treadmill belt at a 20° angle. Thereafter, the belt was turned on for a warm-up session (8 min at 8 m/min). Then, the mice were exercised at 12 m/min for 30 min by downhill running, after which they were returned to their cage. The *mdx* and WT mice ran separately. All mice (including the sedentary mice) were intraperitoneally injected with 1 % (w/v) Evan's blue dye (EBD) at 1 % volume relative to mouse body weight 30 min after the exercise. Exercised *mdx* and WT mice were sacrificed by cervical dislocation 1 day post ($n = 3$) or 5 days post ($n = 3$) exercise. Sedentary (control group, $n = 3$) mice were sacrificed at the same time as the 1 day post exercise mice to assess the EBD infusion into skeletal muscle. These sedentary control mice were housed under standard conditions with no access to voluntary exercise, ensuring minimal physical activity throughout the study period. It should be noted that in one of the mice in the 1 day post exercise group, the level of EBD+ fibers was very low, while extensive muscle damage, necrosis and fibrosis were observed at H&E level in this animal, suggesting that a technical problem could have occurred during the EBD injections. For this reason, the mouse was excluded from the EBD+ analysis.

2.2. Assessment of the exercise-induced muscle damage

After sacrifice, the quadriceps was isolated and sectioned for histological and molecular analyses. Sections of 8 μm were cut with a Leica CM3050 S cryostat (Leica Microsystems B.V. Netherlands) on Superfrost Plus slides (Menzel-Gläzer, Fisher Emergo, Germany). The slides were stored at −80 °C until further use. After warming the slides at room temperature for 30 min, the sections were fixed in ice-cold acetone for 5 min and stained with hematoxylin and eosin and mounted in Pertex mounting medium (HistoLab, Sweden), according to the conventional protocols. Pictures were taken at a 4x magnification using a Pannoramic 250 Flash III whole slide scanner and software (3DHISTECH, Budapest, Hungary). For background correction, Adobe Photoshop version 21.2.11 was used. ImageJ software with the H&E color deconvolution plugin was used for measuring the percentage of unhealthy tissue (consisting of fibrotic and necrotic tissue, recently regenerated fibers and inflammation) in the entire cross section by applying a color deconvolution matrix. These matrices represent the spectral characteristics (color and intensity) of hematoxylin and eosin stains, separating the image into different channels. Each stain has a unique color vector, and the plugin separates them based on their contribution to each pixel's color. (Hematoxylin channel predominantly displays the nuclei. Eosin channel displays the cytoplasm, muscle fibers, and extracellular components. To assess the extent of EBD infusion into skeletal muscle, sections were fixed with ice cold acetone and stained with laminin primary antibody (ab11575, dilution 1:100 Abcam, USA) overnight at 4 °C and with a goat-anti-rabbit Alexa 594 secondary antibody (A11012, dilution 1:1000, Life Technologies) for 1 h at room temperature. Sections were mounted with mounting medium containing DAPI (ProLong Antifade Reagents, Thermo Fischer Scientific). Pictures were taken at a 4x magnification with the fluorescence microscope (Keyence BZ-X700, San Francisco, US). The total area of EBD+ muscle fibers was quantified with ImageJ. Briefly, thresholding was applied to isolate the EBD signal, generating a binary image with Evans Blue-positive areas in white and the background in black. The total Evans Blue Dye uptake area was quantified as a percentage of the total tissue area. Quantification analyses were performed by two examiners blinded to the experimental groups and the mean of the assessments was used for calculations.

2.3. Nanopore cDNA library preparation and sequencing

Total RNA was isolated from the previously sectioned quadriceps samples using TRIsure™ (Bioline, USA) and RNA concentration and purity were measured on the Nanodrop 2000™ (Thermo Scientific, USA). Ribosomal RNA was depleted from the isolated RNA using the Ribo-Zero rRNA Removal Kit (Illumina, *CA*, USA). Then, RNA was purified and concentrated on a RNA Clean Concentrator™−5 column (Zymo Research, Irvine, *CA*, USA). Double stranded cDNA libraries were synthesized using 1 μg of the total RNA using the cDNA kit from Oxford Nanopore Technologies (LSK111, Oxford Nanopore Technologies Ltd, Oxford, UK) with some modifications. Briefly, after synthesis of the 1 strand cDNA synthesis using an oligodT primer we replaced the PCR step with a single extension from the Template Switching Oligo to generate the 2nd strand cDNA. After clean up with Ampure beads the double stranded cDNA were prepared for sequencing using the Native Barcoding kit V14 (Oxford Nanopore Technologies Ltd, Oxford, UK). Nanopore

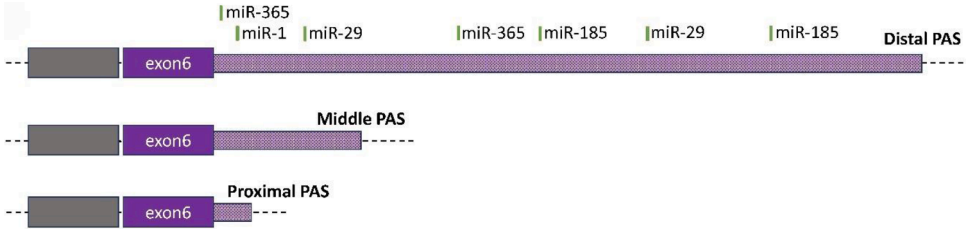

Fig. 1. *Igf1* 3′UTR isoforms. Alternative polyadenylation of the *IGF1* gene and miRNA binding sites [10,13]. The distal PAS gives rise to a ~7 kb long 3′UTR while middle and proximal PASs introduce ~1.2 kb and 200 bp 3′UTRs respectively. PAS: polyadenylation site.

libraries were sequenced using a PromethION P24 with R10 flow cells. The data were generated using MinKNOW 23.04.6 and base calling was performed with Guppy 6.5.7 using the super basecalling model (dna_r10.4.1_e8.2_400bps_sup @v4.2.0). Data analysis was performed following the epi2me-labs/wf-transcriptomes workflow (https://github.com/epi2me-labs/wf-transcriptomes). Briefly, the input files were concatenated to be processed by the workflow with fastcat and trimmed by Pychopper. A reference-guided transcriptome was built for each sample. Then, the reference genome (GRCm39 - mm39) was indexed and sequence alignment was performed using minimap2. The output was converted to BAM files using samtools. For transcript assembly, StringTie was performed with the aligned segments in the chunked BAM files and the output was stored as GFF files. To compare query and reference annotations GffCompare was used. The IGV and UCSC genome browsers were used to visualize the BAM files. For transcript quantification, StringTie (v.2.2.3) was used; the counts were normalized with Deseq2 and normalized counts were used to calculate the relative expression between the *mdx* and WT mice.

2.4. AON design

Igf1 3′UTR (longest) transcript sequence was obtained from the Ensembl genome browser. UCSC Genome browser and PolyApred polyadenylation site predictor (http://crdd.osdd.net/raghava/polyapred/) tools were used to identify the annotated and potential polyadenylation sites. Upstream elements (AU-rich), poly(A) signal sequences and downstream elements (GU-rich) were determined on the distal polyadenylation site that gives rise to a 7 kb long UTR. One AON was designed for each region (Fig. 4A). RNA Structure 6.1 software was used for AON design and evaluation of the physiochemical properties including dimerization and binding energy. All AONs used in the study were produced by Eurogentec, Belgium with 2′-O-methyl phosphorothioate (2OmePS) modifications (Table S1).

2.5. Cell culture and AON transfection

Mouse myoblasts (C2C12, ATCC, Manassas, VA, USA) were cultured in proliferation medium DMEM supplemented with 10 % FBS, 1 % glucose, 2 % glutamax (Thermo Fisher Scientific, Waltham, MA, USA) at 37 °C. When they became fully confluent, medium was replaced with differentiation medium containing 2 % FBS after which they were incubated at 37 °C until the time of transfection. When the myoblast cells started to form myotubes at day 2–3, they were transfected with 200 nM of each AON including a non-targeting control AON (Table S1), using lipofectamine 2000 (2 μl/well) (Thermo Fisher Scientific). For the combinatory use, the total AON concentration was set as 200 nM, with equal quantities of each of the AONs. Transfection was performed in serum free conditions and thereafter, the media was replaced by 2 % serum containing media (Thermo Fisher Scientific, USA) to maintain cell differentiation. Transfected cells were incubated until harvesting time. All transfection experiments were performed with three biological replicates.

2.6. Analysis of alternative polyadenylation redirection on RNA level

Total RNA was isolated at different timepoints after transfection using TRIsure™ (Bioline, USA) and RNA concentration and purity were measured on the Nanodrop 2000™ (Thermo Scientific, USA). For qPCR experiments, isolated RNA was further purified with the NucleoSpin RNA purification kit (Macharey Nagel, Germany). cDNA synthesis was performed with random primers using 1 μg of total RNA followed by qPCR reactions with the primers described in Table S2. qPCR results were analyzed using the CopyCaller v2.1 (Roche Diagnostics, Switzerland) by normalizing to the housekeeping genes *Gapdh* and *Actb*.

2.7. Western blot

For protein extraction of the quadriceps samples, cryosections were collected over the entire tissue during sectioning The slices were treated with 500 μl RIPA lysis buffer in zirconium beads pre-filled tubes and homogenized in Magnalyzer (Roche Diagnostics, Switzerland) for 20 s at speed 7000. Then, the homogenized suspension was transferred to a clean 1.5 ml Eppendorf tube. For *in vitro* experiments, at 48 h after the transfection, C2C12 cells were harvested using 500 μl RIPA lysis buffer from 6-well plates and incubated for 30 min on ice (tissue and cells). After a 10 min centrifugation at 10,000 *g*, protein lysates (supernatant) were transferred to a new tube for further analysis. In total, 50 μg protein was mixed with Laemmli buffer and denatured at 95 °C for 5 min followed by 1 h running on a 4–20 % TGX precast gel (BIO-RAD, USA) at 150 V. Proteins were transferred to a 0.2 μm nitrocellulose membrane (BIO-RAD, USA) using the Trans Blot Turbo system. The membrane was blocked with serum-free blocking buffer (LI-COR, USA) for 1 h and treated with goat-anti-mouse IGF-1 antibody (1:500, AF791, Novus Biologicals, USA), phospho-p44/42 (Erk1/2, 1:3000, #9101), p44/42 (Erk1/2, 1:2000, #9102), phospho-Akt (D9E) XP® (1:3000, #4060), Akt (pan, C67E7, 1:3000, #4691) (Cell Signaling Technology, USA) and GAPDH (1:2000, MAB374, Merck, USA) overnight at 4 °C. The next day, the membranes were washed three times for 10 min with Tris Buffered Saline-Tween (TBS-T) buffer and incubated with the following secondary antibodies in TBS-T for 1 h at room temperature; against the source organisms of the primary antibodies IRDye® 680RD Donkey anti-Goat (1:10,000), IRDye® 680RD Donkey anti-Rabbit (1:10,000), IRDye® 680RD Goat anti-Mouse (1:10,000). After three washing steps in TBS-T, the membrane was visualized and quantified with the Image Studio, Odyssey CLx imaging system (LI-COR Biosciences, Miami USA).

2.8. Illumina library preparation and 3′RNA sequencing

For RNA-seq experiments, isolated RNA from C2C12 cells with four replicates (four wells) was further purified using the NucleoSpin RNA purification kit (Macharey-Nagel, Germany). RNA integrity was checked using the Bioanalyzer2100 (Agilent, *CA*, USA) according to the manufacturer's specifications. The 3′ library preparation was done using oligodT primers, which was followed by NovaSeq6000 Illumina sequencing (GenomeScan, Leiden). The RNA-seq analysis was done with the nf-core rnaseq pipeline (v.3.11.1). Briefly, the adapter sequences, bases with low-quality scores, poly(A) tails, primers and other unwanted sequences were trimmed using the CatAdapt tool (v.4.0). After trimming, FastQC (v.0.12.0) was used to remove low quality bases (Pred score < 33). The trimmed reads were aligned using the STAR alignment tool (v.2.7.3) against the mouse reference genome (GRCm38/mm10).

2.9. Differential expression and pathway analyses

The aligned results were converted to Binary Alignments Map (BAM) files. Then, the feature Counts tool (v2.0.2) was used to quantify each gene feature from each BAM file, producing a final gene count matrix per sample. This data matrix was used as input for quality control analysis in the iDEP.91 environment and also for differential gene expression statistical analysis with Deseq2 (v.1.40.2) to plot differentially expressed genes in volcano plots. In samtools (1.3.1), sorting and indexing were performed to prepare the BAM files for visualization on the UCSC genome bowser. The number of reads that map within a gene was determined for each sample for differential gene expression analysis. The analysis was performed on 10,541 genes for which the average CPM was above 5. We used an R package that contains the R-Shiny application (LUMC/dgeAnalysis v1.5.2) (https://github.com/LUMC/dgeAnalysis). with a Docker (v.23.0.1) image to perform differential gene expression analysis. Once the application initialized in a web browser, the meta data file and the count table that contains the sample information and raw gene counts, respectively were uploaded and the

analyses were performed using Deseq2, Limma/Voom (v.3.20) and EdgeR (v.3.20) with the following cutoff values for a *P*-value = 0.05, log2CPM = 1. To identify biological pathways associated with the differentially expressed genes (DEGs), pathway enrichment analysis was performed. The input gene list was mapped to standard identifiers (Entrez) and analyzed against reference pathway databases, including Reactome, and Gene Ontology (GO) Biological Processes, Molecular Function and Cell Component analyses. Enriched pathways were visualized, and biological relevance was interpreted based on literature and functional annotations.

2.10. Statistical analysis

Data analysis was performed with GraphPad Prism9.3.1 software (GraphPad, San Diego, *CA*, USA) and expressed as means ± SEM. "n" refers to biological replicates as indicated and biological replicates consist of technical triplicates in qPCR experiments. Significance levels were set at * $P < 0.05$, ** $P < 0.01$, *** $P < 0.001$, and **** $P < 0.0001$.

The amounts of EBD+ fibers and percentage of unhealthy tissue in exercised/sedentary *mdx* and WT mice were assessed by one-way analysis of variance (ANOVA) followed by Bartlett's correction and Tukey's multiple comparison. The relative expressions of *Igf1* and its 3′UTR in the exercised/sedentary *mdx* and WT mice were assessed with a two-way ANOVA followed by Sidak's multiple comparison (*Igf1*) and Tukey's multiple comparison (3′UTRs). Relative distal polyadenylation site usage and abundancy of *Igf1* 3′UTRs after AON transfection, were assessed by one-way ANOVA followed by Bartlett's correction and Tukey's multiple comparison.

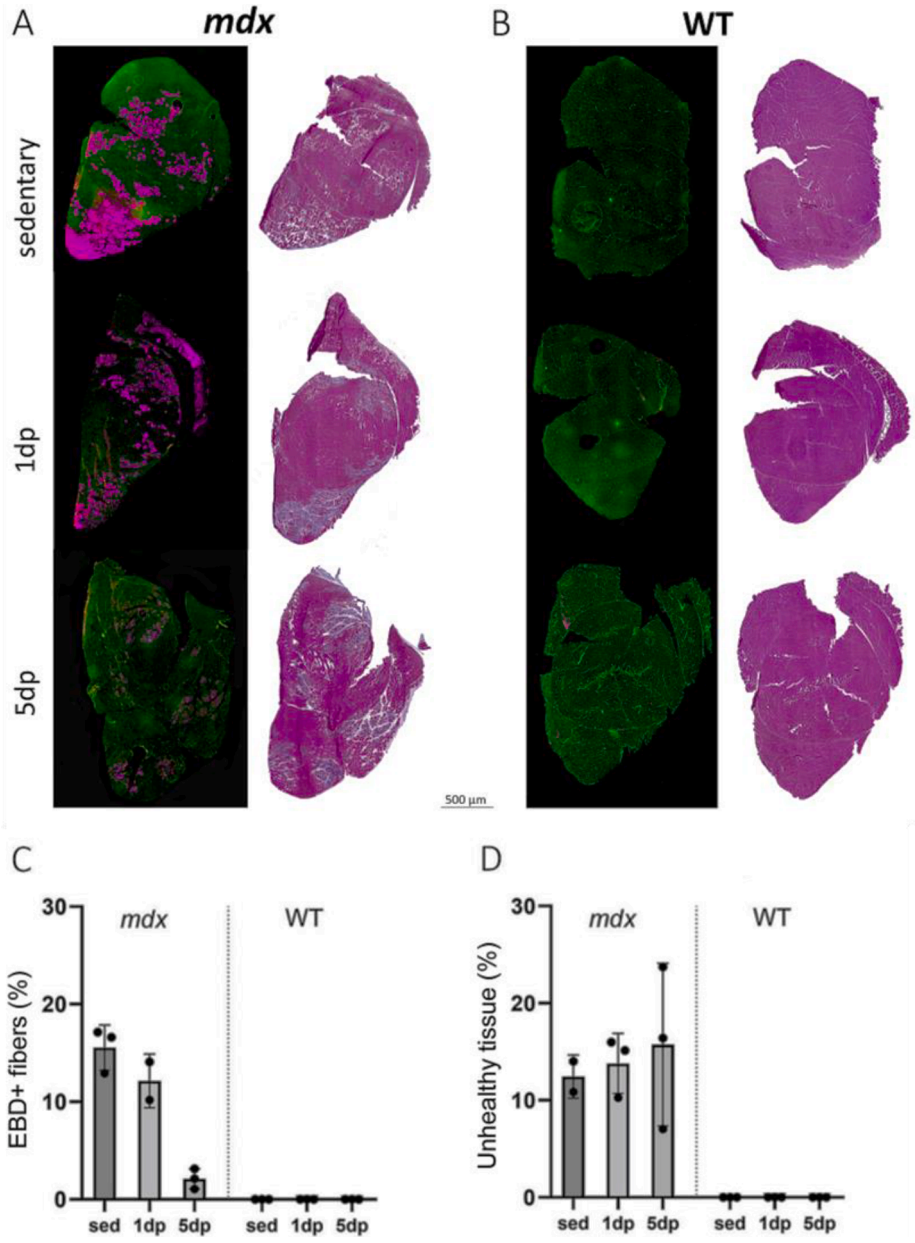

Fig. 2. Histological analysis of the quadriceps muscles after downhill treadmill running in *mdx* and WT mice. EBD, (pink), laminin (green) and H&E staining results of the *mdx* (A) and wild type (WT) (B) quadriceps. Representative images are shown as paired for each group. C. Bar graph showing the EBD+ fiber levels in sedentary, 1dp and 5dp groups of the *mdx* mice. No EBD+ fibers were detected in wild type muscles. D. Quantification of areas of unhealthy tissue (fibrosis, necrosis, inflammation) in sedentary, 1dp and 5dp groups of the *mdx* and WT mice. No pathology was observed in the WT mice. $n = 3$ per group, one-way ANOVA (followed by Sidak's multiple comparison) comparing EBD+ fibers or unhealthy tissue (%) among different groups. All data are plotted as means ± SEM. Sed: sedentary, 1dp: 1 day post exercise, 5dp: 5 days post exercise.

3. Results

3.1. Downhill running exercise redirects Igf1 3′UTRs towards the proximal polyadenylation site in wildtype mice only

We utilized a single 30 min downhill treadmill exercise, which is known to induce muscle damage and associated molecular and cellular changes in *mdx* mice [14], to assess whether *Igf1* 3′UTRs are differentially utilized in response to exercise and muscle dystrophy. Thirty minutes after the exercise, mice were injected with EBD to quantify damaged muscle fibers in the quadriceps given that it is one of the most severely affected muscles in downhill exercises [14]. The exercised mice (both *mdx* and WT) were either sacrificed at 1 or 5 days post exercise and compared to sedentary mice (Fig. 2A and B).

For the *mdx* mice, a large number of EBD+ fibers was observed 1 day post exercise, while the signal was much reduced in the 5 days post mice as reported previously (Fig. 2A–C) [15] . However, we also observed a large number of EBD+ fibers in sedentary *mdx* mice (Fig. 2A–C). In the H&E analysis, no significant difference was observed between the exercised and sedentary *mdx* mice with regards to visual appearance of fibrosis and necrosis, while high variation was observed between the 5 days post exercise mice (Fig. 2D). No pathology was observed in the WT quadriceps muscles (Fig. 2B–D).

To study how exercise influenced *Igf1* 3′UTR site choice, we isolated RNA from quadriceps muscles and analyzed transcripts with Nanopore cDNA-seq.

After sequencing and transcript quantification, we first analyzed the overall *Igf1* expression in *mdx* and WT mice upon exercise and found that *Igf1* expression was higher in the *mdx* mice compared to WT mice before and after the exercise (Fig. 3A). However, downhill running did not significantly increase *Igf1* expression in any of the strains. Although higher *Igf1* expression levels were observed in exercised WT mice, this was not significant due to the variation between mice (Fig. 3A), pointing out the need of more biological replicates to draw a conclusion. Then, we investigated the distribution of *Igf1* 3′UTR isoforms in *mdx* and WT mice using the isoform specific transcript counts. In the *mdx* mice, the exercise did not affect the *Igf1* 3′UTR pattern, which was already shifted to the proximal polyadenylation site before the exercise (Fig. 3B). On the other hand, in the WT mice, there was a clear shift from the distal polyadenylation site to the proximal polyadenylation site, while the middle polyadenylation site remained almost unchanged at both 1 day and 5 days post exercise mice (Fig. 3B).

Further, we studied the effect of the exercise on IGF-1 protein levels in the quadriceps muscles of the *mdx* and WT mice by performing a Western blot analysis. First, we found that the baseline IGF-1 level (in sedentary mice) was higher in the *mdx* mice compared to the WT IGF-1 levels (Fig. 3C and D). At 1 day post exercise groups, IGF-1 levels were found to be significantly decreased in the *mdx* mice, while this was

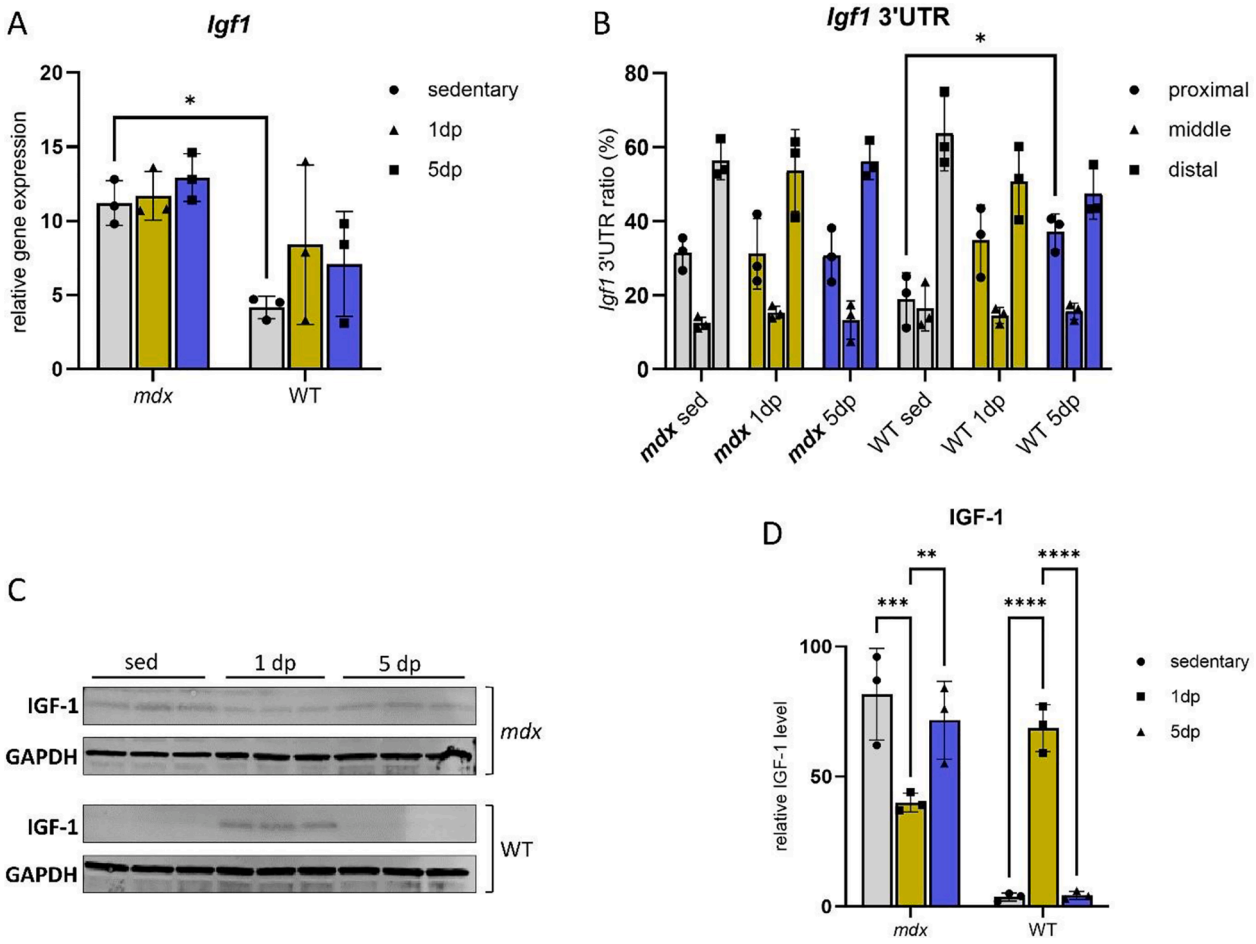

Fig. 3. Investigation of *Igf1* 3′UTR pattern in dystrophic and exercised conditions. A. Bar graph comparing the *Igf1* gene expression levels of the *mdx* and the WT mice in sedentary and exercised conditions based on the normalized transcript counts. B. Bar graph showing the ratios of *Igf1* 3′UTRs relative to total *Igf1* levels, in sedentary/exercised *mdx* and WT mice. C-D. Blots and bar graphs showing the IGF-1 (~17 kDa) protein levels in exercised *mdx* and WT quadriceps (GAPDH as loading control). $n = 3$ replicates, * $P < 0.05$, ** $P < 0.01$, *** $P < 0.001$, **** $P < 0.0001$, two-way ANOVA comparing relative expression levels of *Igf1*/IGF-1 (Sidak's multiple comparison) and the ratios of *Igf1* 3′UTRs (Tukey's multiple comparison) in sedentary/exercised *mdx* and WT mice. All data are plotted as means ± SEM. PAS: polyadenylation site, 1dp: 1 day post exercise, 5dp: 5 days post exercise.

dramatically increased in the WT mice. Interestingly, at 5 days post exercise, IGF-1 levels were elevated in the *mdx* mice, whereas a sharp reduction was observed in the WT mice. Taken together, the downhill treadmill running protocol had a different impact on IGF-1 levels in the *mdx* and WT mice.

3.2. Distal polyadenylation site targeting AONs redirect Igf1 APA

Based on our exercise study, we speculated that shifting *Igf1* 3′UTR usage towards the proximal or middle polyadenylation site would result in increased IGF-1 protein expression [10]. To induce this shift, we designed three different AONs targeting the cis-regulatory elements involved in polyadenylation and cleavage: AU-rich upstream elements that typically enhance poly(A) site recognition, the poly(A) signal sequence, which is essential for polyadenylation complex recruitment and GU-rich downstream elements that interacts with CPSF and CstF complexes to stabilize cleavage at the poly(A) site. The names of the AONs were given based on these elements (AU-rich upstream elements (USE), poly(A) signal (SIG), GU-rich downstream elements (DSE)) (Fig. 4A). As AON transfection can influence cell differentiation, we used a control AON as a reference. Transfection of C2C12 myoblasts was performed at day 2 in differentiation media (just before differentiation) and the cells were harvested after 24 h and 48 h for RNA and protein isolations, respectively. The qPCR analysis showed a reduced level of the distal 3′UTR in cells treated with the distal polyadenylation site targeting AONs compared to the control AON treated cells (Fig. 4B). Importantly, total *Igf1* transcript levels remained the same during the AON treatment (Fig. 4C). At 36 h, the redirection was less visible in all conditions, while the cells started to differentiate (Supplemental Figure S1). AON SIG was selected as the lead AON for further experiments.

Next, we studied the possible effect of the APA redirection on protein level. In AON SIG treated cells, IGF-1 levels were found to be increased compared to the control AON treated cells. In addition to this, AKT phosphorylation, one of the main targets in IGF-1 signaling, was also elevated (Fig. 4D–F), while total AKT levels remained unchanged (Fig. 4E and F).

3.3. Igf1 APA redirection altered expression of genes related to myogenesis and calcium homeostasis

Given that *Igf1* distal polyadenylation site targeting might affect IGF-1 signaling and cell differentiation, we decided to further analyze the related transcriptome and quantify the *Igf1* 3′UTR in AON SIG treated cells by performing 3′ RNA sequencing. For this, C2C12 cells were transfected with AON SIG or a control AON at day 2 of differentiation as before and we isolated RNA 36 h post transfection as we observed that the effect of polyadenylation site redirection started to decrease between 24 and 36 h.

Once the raw data was obtained, cleaning and quality control analyses were performed, and the reads were aligned to the mouse reference genome (GRCm39/mm39). Here, 86 % of transcripts were found to be uniquely mapped. For each condition, four replicates were used, and they clustered together per condition (Fig. 5A). After filtering, differentially expressed gene analysis was performed by DESeq2, limma-voom

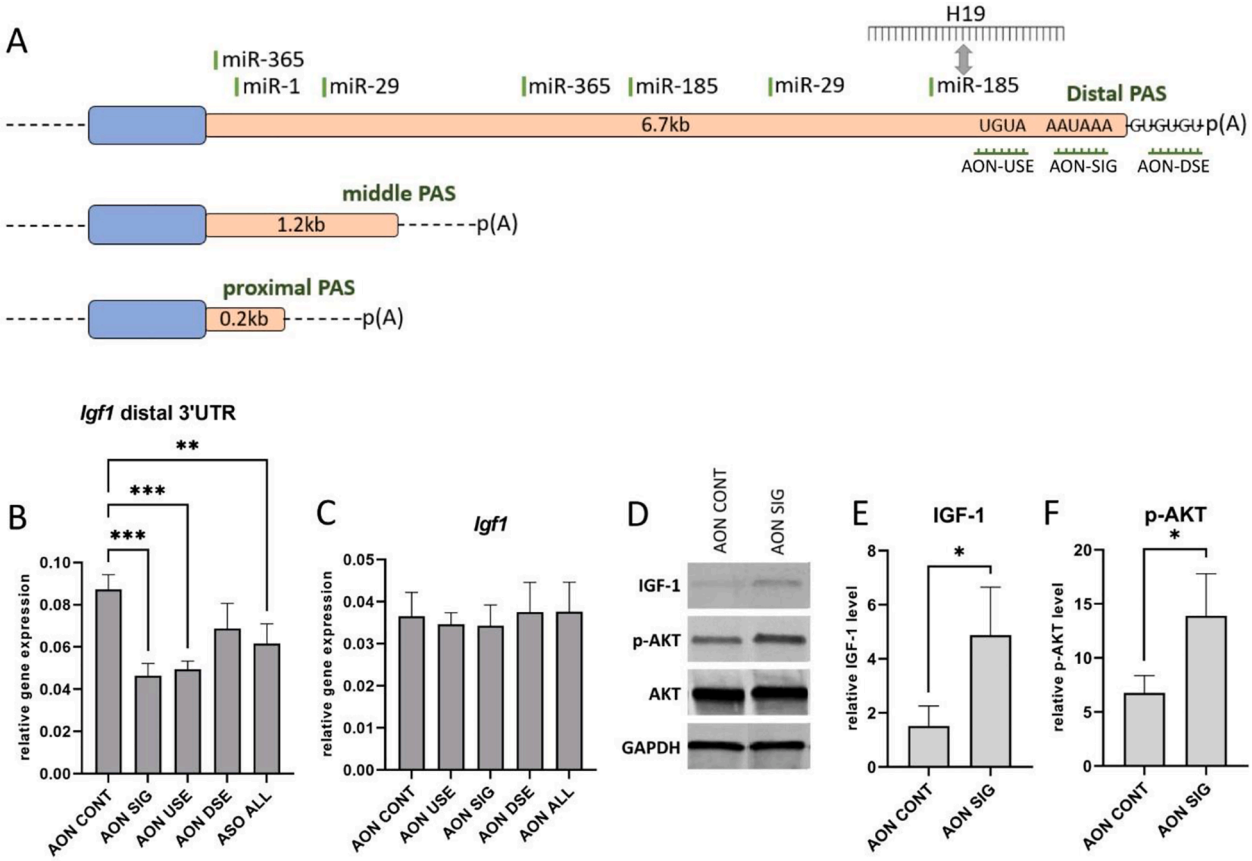

Fig. 4. AON-mediated redirection of *Igf1* APA. A. Schematic representation of *Igf1* 3′UTRs, miRNA target sites and AONs targeting the distal polyadenylation site. Bar graphs showing relative expressions of *Igf1* distal 3′UTR in C2C12 cells treated with the distal PAS targeting AONs (B) and total *Igf1* (C). D. Western blots of IGF-1, p-AKT and AKT (GAPDH as loading control) in C2C12 cells treated with AON SIG and control AON. All blots are a representative of three independent Western blot experiments. $n = 3$ replicates, ** $P < 0.01$, *** $P < 0.001$, one-way ANOVA (followed by Sidak's multiple comparison) comparing relative expression levels between the distal PAS targeting AONs and the control AON. All data are plotted as means ± SEM. PAS: polyadenylation site. p(A): polyadenylation. AON ALL: combinatory use with equal quantities of each of the AONs.

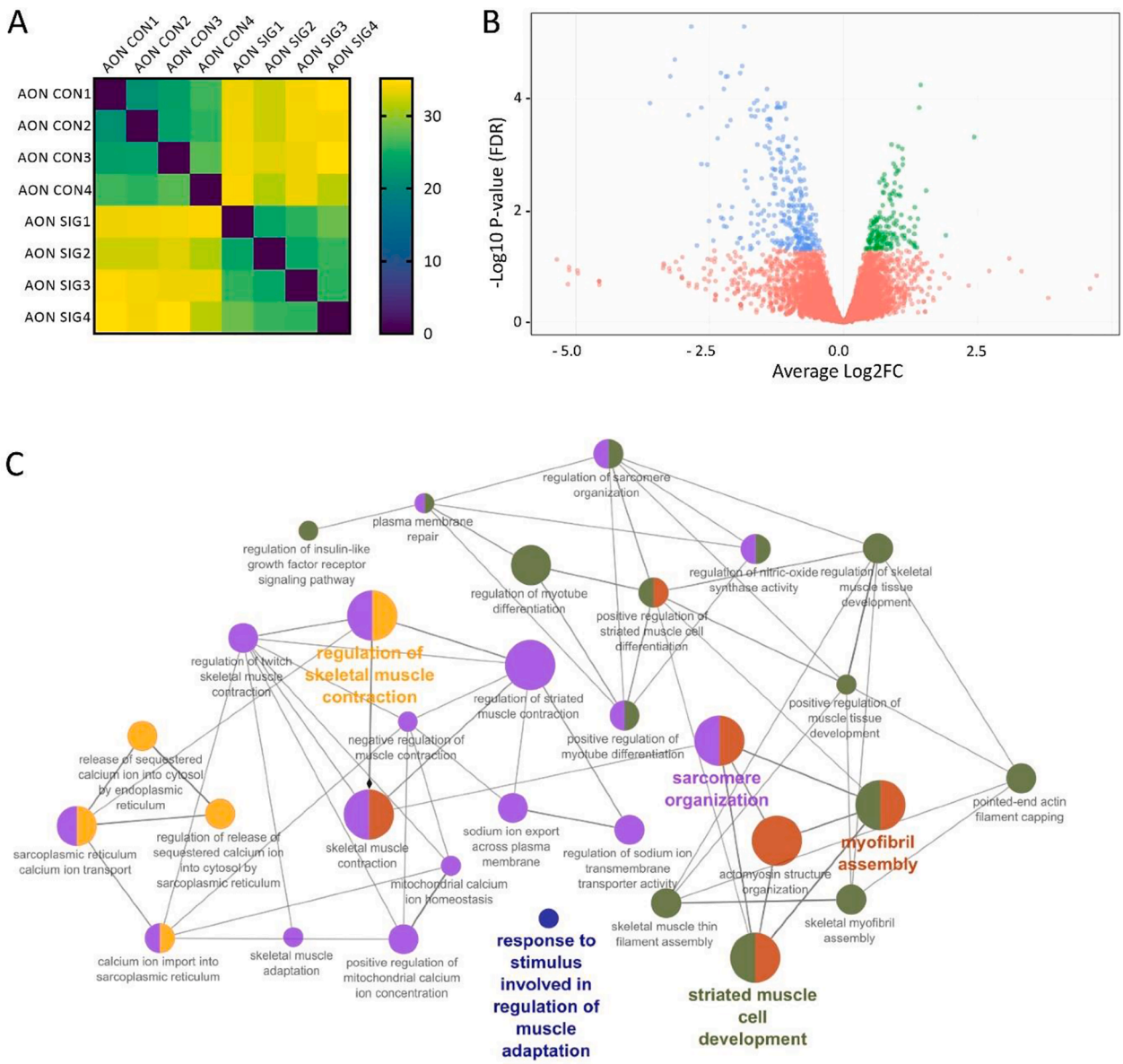

Fig. 5. Differential gene expression analysis. A. Heatmap showing the gene expression data for AON SIG treated and control AON treated cells (four replicates). Hierarchical clustering of samples represents the distances across samples. B. Volcano plot showing the difference in gene expression levels between AON SIG treated and control AON treated cells. The log2FC is plotted on the x-axis, while the −log10 of the adjusted *P*-value is plotted on the y-axis. Green dots are upregulated genes, blue dots are downregulated genes while red dots are non-DEGs (adjusted $P < 0.05$). C. Gene-concept network analysis showing the connection between the enriched terms. The node size correlates to the term enrichment significance.

and edgeR and all three tools reported around ~300 downregulated and ~150 upregulated genes in AON SIG treated cells compared to the control AON treated cells (Fig. 5B). The gene network analysis revealed which genes are involved in the most significant terms as well as their connection with the associated genes and terms (Fig. 5C). GO annotations of the DE genes showed a strong enrichment for genes involved in sarcomere organization, calcium homeostasis, regulation of skeletal muscle contraction and muscle cell development (Fig. 6A). GO cellular component analysis showed the macromolecular complexes and subcellular structures related to muscle structure and development (Fig. 6B). Molecular function analysis mapped the majority of the genes to cytoskeletal protein binding and ion binding (Fig. 6C). Most of the genes represented in these GO terms were found to be downregulated. Examples of downregulated genes in AON SIG treated cells were *Tcap, Myh1, Myh3, Myh4, Myh7, Casq1, Trim72, Cd36, Myom3, Myl1, Myl4, Car3, Mb* and *Mef2c*, which are all known to be involved in myogenic differentiation. Upregulated genes in response to the redirection of the APA included *Stmn1, Cdkn1* and *Igfbp5*.

3.4. Internal poly(A) and poly(T) tract introduce a systematic bias on quantification and coverage

Using the 3′UTR data, we also tried to quantify the 3′ ends of *Igf1*, but this resulted in a less prominent shift compared to what was previously found by qPCR analysis (Fig. 7A and B). For a more detailed investigation, we generated the BAM files using samtools and visualized them in the IGV genome browser. Besides the peaks aligning with the annotated polyadenylation sites, there were three other strong peaks between the middle and the distal polyadenylation site (Fig. 7C). Once the sequences of these regions were obtained, we recognized the presence of the internal adenine (A) and thymine (T) runs that can be targeted by oligo (dT) primers during the first strand and/or second strand cDNA

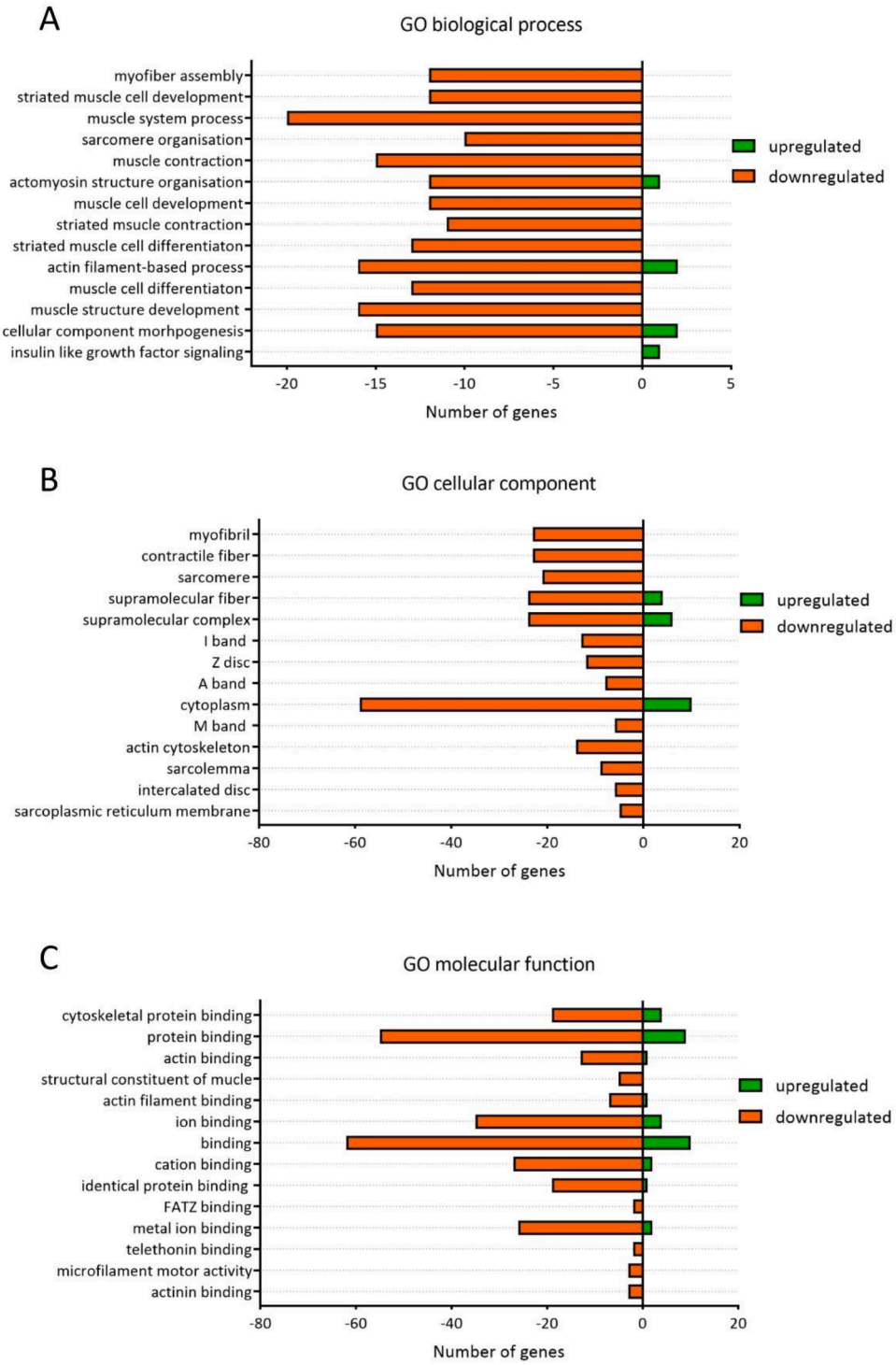

Fig. 6. GO enrichment analysis for the DEGs. A. Bar graph showing the results of GO biological process analysis. B. Bar graph showing the results of GO cellular component analysis. C. Bar graph showing the results of GO molecular function analysis. Statistically most significant results are given from top to bottom order in each graph.

synthesis. The read cluster with blue color represents the reads generated from the negative strand containing a T-stretch on the mRNA. This T-stretch is then converted to A-stretch during the first strand cDNA synthesis and targeted by oligo(dT) primers. The abundance of these transcripts is over-estimated in the presence of oligodT priming, at the expense of the other transcripts [16].

This bias and the internal A-stretches not only affect quantification, but also the read length for Nanopore cDNA-seq full-length transcriptome sequencing. While the internal A-runs result in 3′-truncation of the cDNA, the internal T-runs on transcripts transcribed from the opposite strand, during 2nd strand cDNA synthesis, lead to 5′-truncation of the cDNA.

Because the cDNA was synthesized using random hexamer primers in the qPCR analysis of the distal polyadenylation site along with the total *Igf1* transcript levels (in the AON study), this quantification was not influenced by the presence of internal A and T-runs as we observed

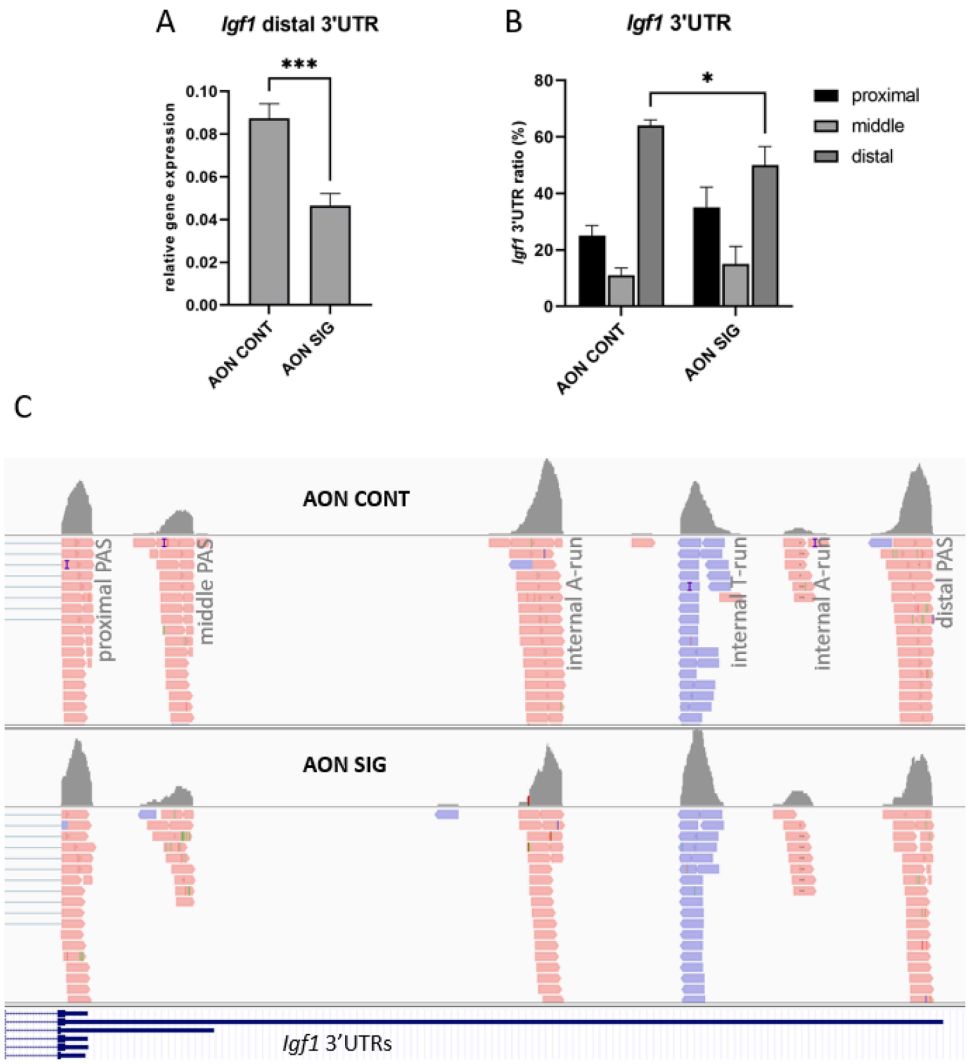

Fig. 7. Internal oligo(dT) priming issue on the *Igf1* 3′ ends. A. Quantification of the *Igf1* distal 3′UTR by qPCR in AON SIG treated cells. B. *Igf1* 3′UTR ratios measured by 3′sequencing in AON SIG treated cells. For calculation, the sum of the three PASs is taken as 100 and individual PAS percentages were calculated based on their relative abundancies. C. Picture taken from IGV/UCSC genome browsers showing the BAM file visualization of the AON SIG treated and the control AON treated (top) cells. Pink lines represent the reads that belong to the coding strand while the blue lines represent the reads from the non-coding strand. *Igf1* 3′UTRs and their polyadenylation sites coordinates are given at the bottom. $n = 3$ replicates. Panel A, a one-way ANOVA comparing relative expression levels of *Igf1* distal 3′UTR, for panel B a two-way ANOVA comparing the ratios of *Igf1* 3′UTRs in AON SIG and AON CONT treated cells, followed by Sidak's multiple comparison tests. All data in panel A and B are plotted as means ± SEM. * $P < 0.05$, *** $P < 0.001$.

during the analyses of the Nanopore cDNA-seq and 3′-seq data.

4. Discussion

IGF-I is an important growth factor for proliferation and differentiation of skeletal muscle cells and therefore IGF-1 treatment has been considered as a therapy for DMD [17]. In *mdx* mice, strategies to enhance IGF-1 signaling—via local or systemic administration and muscle-specific expression—have improved muscle regeneration and strength, and reduced apoptosis [18–20]. However, route of administration, timing of injection, dose/duration of the treatment, onset of disease pathology and the animal model used may affect the actions of IGF-1 in skeletal muscle. While local IGF-1 overexpression increases muscle mass in *mdx* mice, systemic recombinant IGF-1 does not, likely due to its sequestration by IGF-binding proteins (IGFBPs). PEGylated IGF-1 has shown benefits in young *mdx* mice but limited effects in older or severely affected dystrophic models, highlighting the need for alternative strategies [21,22]In this study, we investigated the 3′UTR isoforms of the *Igf1* gene in exercised *mdx* and WT mice and developed an AON-mediated approach to increase IGF-1 protein levels in C2C12 cells by redirecting the *Igf1* APA towards the upstream polyadenylation sites to generate more stable *Igf1* transcripts. Related transcriptome changes following the AON treatment were unraveled by 3′RNA sequencing.

To investigate the effect of downhill running exercise on *Igf1* expression and the distribution of the 3′UTRs in *mdx* and WT mice, we performed a full-length transcript sequencing, and our first observation was that in the sedentary *mdx* mice overall *Igf1* mRNA expression and relative usage of the proximal polyadenylation site was found to be significantly higher compared to the sedentary WT. This might be attributed to the ongoing regeneration in *mdx* mouse muscle [23,24]. On the other hand, no significant change was observed in *mdx* and WT mice upon exercise in overall *Igf1* gene expression despite the relative increase in exercised WT mice with very high variation between mice. After the exercise, *Igf1* 3′UTR was shifted towards the proximal polyadenylation site in WT mice, whereas it did not significantly change in the *mdx* mice. One could speculate that *mdx* mice already have relatively more proximal polyadenylation site usage and that the downhill exercise was not enough to make additional changes on 3′UTRs usage, but it is

also possible that other factors related to the ongoing muscle pathology in *mdx* mice played a role. Analysis of IGF-1 protein levels in the exercised *mdx* and WT mice showed that IGF-1 levels are significantly higher in the *mdx* mice compared to the WT mice in the sedentary condition. Because the total *Igf1* levels are higher in the *mdx* mice compared to the WT, to what extent the higher proximal polyadenylation site usage in the *mdx* mice contributed to the higher IGF-1 protein levels remains unclear. Despite the stable *Igf1* mRNA levels in the 1 days post exercise *mdx* mice, we observed a reduction on IGF-1 protein levels in that group. Given the unchanged pattern of the *Igf1* 3′UTRs in these mice, this could be due to the other regulatory factors that could bind the 3′UTR, such as downregulatory miRNAs and RNA binding proteins. In the WT mice, the downhill exercise caused a very sharp increase in IGF-1 levels at day 1. Since the *Igf1* mRNA levels were not significantly affected by the exercise, we speculate that the higher proximal polyadenylation site usage observed in the 1 day and 5 days post exercise WT mice could be one of the reasons for this increase. On the other hand, very low levels of IGF-1 were observed in the 5 days post exercise WT mice despite a persistent higher proximal polyadenylation site usage on transcript level. It should also be considered that the quadriceps IGF-1 levels might have been affected by the liver-derived IGF-1 levels in an endocrine manner. Therefore, it remains challenging to draw a conclusion about the relation between the redirected APA and the IGF-1 protein levels in the exercised *mdx* and WT mice.

While our initial rationale for employing nanopore long-read sequencing was to explore potential connectivity between the *Igf1* alternative polyadenylation and alternative splicing events in response to downhill treadmill exercise, technical limitations, particularly internal A/T-rich stretches, impaired full-length cDNA synthesis and restricted our ability to fully assess transcript connectivity. As a result, the long-read data did not provide substantially more insight beyond what was achievable with 3′-seq for polyadenylation site quantification. To minimize the internal oligodT priming issue that led to truncated reads in our nanopore cDNA-seq analysis, future studies could incorporate biotinylated capture beads targeting a common exon present in all *Igf1* isoforms (exon 3 or 4 in this case).

AONs can modulate polyadenylation by targeting polyadenylation signals or other *cis*-regulatory elements for the purposes of gene knockdown [25,26] or redirection of APA to favor the utilization of a preferred transcript [27]. In this study, we redirected *Igf1* APA to the upstream polyadenylation sites by an AON-mediated approach and this resulted in increased IGF-1 protein expression and the downstream signaling in C2C12 cells. To our knowledge, this is the first demonstration of the use of AONs to increase IGF-1 levels without modifying the coding region. However, it should be noted that the phenotypic difference caused by the differentiation might have contributed to the elevated IGF-1 levels as well. It was observed that overall *Igf1* transcript levels were not changed after the AON treatment while IGF-1 protein levels found to be increased compared to the control. We speculate that the dynamics of gene transcription and translation causes the differences between panel D and E. The protein effect will happen later than the transcript effect, so it is possible that the transcript levels have already gone back to normal while the protein effect and signaling effects linger. Furthermore, translation efficiency and miRNA-mediated translation repression might have contributed the differences observed on RNA and protein levels. The AON-SIG treatment reduces the usage of the distal polyadenylation site, resulting in shorter transcripts. The mRNA-protein discrepancy observed in the study could have been caused by the changes in mRNA isoform composition that might enhance translation, rather than total mRNA abundance. Given that the *cis*-regulatory elements on the distal polyadenylation site may be dispensable, we also used all AONs in combination, but this led to a lower reduction on the distal polyadenylation site usage compared to the AON USE and AON SIG. It seems that targeting the upstream elements and the polyadenylation signal provides a more prominent redirection. Presumably, a more efficient redirection could be achieved by higher concentrations in combinatory use when we consider the relatively lower Tm and binding energy due to the AU-rich regions around the distal polyadenylation site.

The *Igf1* APA shift in C2C12 cells resulted in a change in transcripts involved in muscle-associated pathways, most importantly in sarcomere organization, muscle cell development, muscle contraction and calcium homeostasis. A number of genes related to myoblast differentiation was found to be downregulated. Among the genes in the IGF-1 axis, only *Igfbp5* was differentially upregulated. IGFBP5 is the most abundant IGF binding protein in skeletal muscle and it can modulate IGF-1 activity via several mechanisms, for example by competing with IGF-1R to inhibit IGF-1 actions, or in an opposite function, it can sequester IGF-1 around the receptor in skeletal muscle, thereby enhancing signaling [28]. Therefore, IGFBP5 upregulation could be due to a feedback mechanism in response to elevated IGF-1 expression Moreover, *Tcap*, a key player in sarcomere stability, and several myosin heavy chain genes (*Myh1, Myh3, Myh4, Myh7*) were differentially expressed, reflecting IGF-1′s role in muscle fiber adaptation and repair. Additionally, *Casq1* and *Trim72*, both involved in calcium homeostasis and muscle repair, showed altered expression. This suggests IGF-1′s critical role in maintaining calcium balance and membrane integrity, as noted by others [29]. We also observed changes in *Cd36*, a fatty acid transporter, pointing to IGF-1′s involvement in muscle metabolism. *Mef2c, Igfbp5*, and genes related to muscle stem cell regulation (*Stmn1, Cdkn1, Myl1*) further suggest IGF-1′s role in muscle differentiation, regeneration, and cell cycle progression.

IGF-1 isoform expression varies not only between tissues but also across species, which may impact the translational potential of AON-mediated approaches targeting the 3′UTR [30]. Differences in IGF-1 regulation, APA patterns, and RNA-binding protein interactions across species could influence the effectiveness of such strategies. For example, human and rodent IGF-1 isoforms exhibit distinct expression profiles and regulatory elements, meaning findings in model organisms may not fully translate to human applications. This species specificity should be carefully considered when designing therapeutic interventions to ensure their applicability across different biological systems.

While our current study is limited to *in vitro* experiments, these systems provide a proof of principle to modulate *Igf1* alternative polyadenylation. Importantly, the use of AONs to modulate polyadenylation has been validated *in vivo* in other context [25], supporting the potential translatability of this strategy. Future studies will be needed to explore the physiological relevance and therapeutic feasibility of targeting *Igf1* polyadenylation *in vivo*.

In conclusion, we investigated the patterns of *Igf1* 3′UTRs in the exercised *mdx* and WT mice and developed an AON-mediated approach to increase IGF-1 protein expression by redirecting the APA towards the upstream polyadenylation sites. Given that most mammalian genes have multiple polyadenylation sites, it is likely that many other targets with therapeutic potential could be studied with this strategy. Moreover, APA plays a role in other pathologies, particularly in various muscle disorders, where dysregulation of polyadenylation can impact gene expression and disease progression [31]. Understanding APA's broader implications may provide new avenues for therapeutic intervention in muscle-related and other diseases.

Datasets/data availability statement

The data supporting the findings of this study are openly available in NCBI BioProject database PRJNA1074229 (3′RNA sequencing by Illumina), PRJNA1074311 (Full-length transcript sequencing by Oxford Nanopore).

CRediT authorship contribution statement

Alper Yavas: Writing – review & editing, Writing – original draft, Validation, Software, Methodology, Formal analysis, Data curation, Conceptualization. **Maaike van Putten:** Writing – review & editing,

Supervision, Conceptualization. **Yavuz Ariyurek:** Software, Methodology. **Annemieke Aartsma-Rus:** Writing – review & editing, Visualization, Supervision, Project administration, Investigation, Conceptualization.

Declaration of competing interest

The authors declare the following financial interests/personal relationships which may be considered as potential competing interests:

Alper Yavas reports financial support was provided by Leiden University Medical Center. Alper Yavas reports a relationship with Leiden University Medical Center that includes: employment. Annemieke Aartsma-Rus reports a relationship with Leiden University Medical Center that includes: board membership, consulting or advisory, employment, funding grants, speaking and lecture fees, and travel reimbursement. Maaike van Putten reports a relationship with Leiden University Medical Center that includes: employment. Yavuz Ariyurek reports a relationship with Leiden University Medical Center that includes: employment. Annemieke Aartsma Rus discloses being employed by LUMC which has patents on exon skipping technology, some of which has been licensed to BioMarin and subsequently sublicensed to Sarepta. As co-inventor of some of these patents AAR was entitled to a share of royalties. AAR further discloses being ad hoc consultant for PTC Therapeutics, Sarepta Therapeutics, Regenxbio, Alpha Anomeric, Lilly BioMarin Pharmaceuticals Inc., Eisai, Entrada, Takeda, Splicesense, Galapagos and Astra Zeneca. Past ad hoc consulting has occurred for: CRISPR Therapeutics, Summit PLC, Audentes Santhera, Bridge Bio, Global Guidepoint and GLG consultancy, Grunenthal, Wave and BioClinica. AAR also reports having been a member of the Duchenne Network Steering Committee (BioMarin) and being a member of the scientific advisory boards of Eisai, hybridize therapeutics, silence therapeutics, Sarepta therapeutics and MitoRx. Past SAB memberships: ProQR, Philae Pharmaceuticals. Remuneration for these activities is paid to LUMC. LUMC also received speaker honoraria from PTC Therapeutics, Alnylam Netherlands, Pfizer and BioMarin Pharmaceuticals and funding for contract research from Italfarmaco, Sapreme, Eisai, Galapagos, Synnaffix and Alpha Anomeric. Project funding is received from Sarepta Therapeutics and Entrada. Alper Yavas, Maaike van Putten and Yavuz Ariyurek declare that they have no conflict of interest. If there are other authors, they declare that they have no known competing financial interests or personal relationships that could have appeared to influence the work reported in this paper.

Acknowledgments

Several authors of this publications are members of The Netherlands Neuromuscular Center, the Duchenne Centrum Netherlands, and the European Reference Network for rare neuromuscular diseases EURO—NMD. This work was supported by the Duchenne Parent Project and the LUMC Human Genetics department funding.

Supplementary materials

Supplementary material associated with this article can be found, in the online version, at doi:10.1016/j.nmd.2025.105394.

References

[1] Mendell JR, Lloyd-Puryear M. Report of MDA muscle disease symposium on newborn screening for Duchenne muscular dystrophy. Muscle Nerve 2013;48(1):21–6. https://doi.org/10.1002/mus.23810. Epub 2013/05/30PubMed PMID: 23716304.

[2] Mozin E., Massouridès E., Mournetas V., Lièvre C., Bourdon A., Jackson D.L., et al. Dystrophin deficiency impairs cell junction formation during embryonic myogenesis. bioRxiv. 2023. Epub 2023/12/18. doi: 10.1101/2023.12.05.569919. PubMed PMID: 38106055; PubMed Central PMCID: PMCPMC10723310.

[3] Guiraud S, Davies KE. Regenerative biomarkers for Duchenne muscular dystrophy. Neural Regen Res 2019;14(8):1317–20. https://doi.org/10.4103/1673-5374.253534. Pmid 30964048PubMed PMID: WOS:000471039600004.

[4] Spinazzola JM, Kunkel LM. Pharmacological therapeutics targeting the secondary defects and downstream pathology of Duchenne muscular dystrophy. Expert Opin Orphan Drugs 2016;4(11):1179–94. https://doi.org/10.1080/21678707.2016.1240613. PubMed PMID: WOS:000386809800009.

[5] Ahmad SS, Ahmad K, Lee EJ, Lee YH, Choi I. Implications of insulin-like growth factor-1 in skeletal muscle and various diseases. Cells 2020;9(8). https://doi.org/10.3390/cells9081773. ARTN 1773PubMed PMID: WOS:000564689400001.

[6] Song Y-H, Song JL, Delafontaine P, Godard MP. The therapeutic potential of IGF-I in skeletal muscle repair. Trends Endocrinol Metab 2013;24(6):310–9. https://doi.org/10.1016/j.tem.2013.03.004. Epub 2013/04/27PubMed PMID: 23628587.

[7] Gehrig SM, van der Poel C, Hoeflich A, Naim T, Lynch GS, Metzger F. Therapeutic potential of PEGylated insulin-like growth factor I for skeletal muscle disease evaluated in two murine models of muscular dystrophy. Growth Horm IGF Res 2012;22(2):69–75. https://doi.org/10.1016/j.ghir.2012.02.004. Epub 2012/03/20PubMed PMID22424862.

[8] Philippou A, Barton ER. Optimizing IGF-I for skeletal muscle therapeutics. Growth Horm IGF Res 2014;24(5):157–63. https://doi.org/10.1016/j.ghir.2014.06.003. Epub 20140619PubMed PMID: 25002025; PubMed Central PMCID: PMCPMC4665094.

[9] Elkon R, Ugalde AP, Agami R. Alternative cleavage and polyadenylation: extent, regulation and function. Nat Rev Genet 2013;14(7):496–506. https://doi.org/10.1038/nrg3482. Epub 2013/06/19PubMed PMID: 23774734.

[10] Smith SS, Kessler CB, Shenoy V, Rosen CJ, Delany AM. IGF-I 3′ untranslated region: strain-specific polymorphisms and motifs regulating IGF-I in osteoblasts. Endocrinology 2013;154(1):253–62. https://doi.org/10.1210/en.2012-1476. Epub 20121126PubMed PMID: 23183171; PubMed Central PMCID: PMCPMC3529377.

[11] Shepard PJ, Choi EA, Lu J, Flanagan LA, Hertel KJ, Shi Y. Complex and dynamic landscape of RNA polyadenylation revealed by PAS-Seq. Rna 2011;17(4):761–72. https://doi.org/10.1261/rna.2581711. Epub 2011/02/24PubMed PMID: 21343387; PubMed Central PMCID: PMCPMC3062186.

[12] Wu Y, Jiang Y, Liu Q, Liu CZ. lncRNA H19 promotes matrix mineralization through up-regulating IGF1 by sponging miR-185-5p in osteoblasts. BMC Mol Cell Biol 2019;20(1):48. https://doi.org/10.1186/s12860-019-0230-3. Epub 2019/11/14PubMed PMID: 31718549; PubMed Central PMCID: PMCPMC6852999.

[13] Elia L, Contu R, Quintavalle M, Varrone F, Chimenti C, Russo MA, et al. Reciprocal regulation of microRNA-1 and insulin-like growth factor-1 signal transduction cascade in cardiac and skeletal muscle in physiological and pathological conditions. Circulation 2009;120(23):2377–85. https://doi.org/10.1161/circulationaha.109.879429. Epub 20091123PubMed PMID: 19933931; PubMed Central PMCID: PMCPMC2825656.

[14] Radley-Crabb H, Terrill J, Shavlakadze T, Tonkin J, Arthur P, Grounds M. A single 30min treadmill exercise session is suitable for 'proof-of concept studies' in adult mdx mice: a comparison of the early consequences of two different treadmill protocols. Neuromuscul Disord 2012;22(2):170–82. https://doi.org/10.1016/j.nmd.2011.07.008.

[15] Hamer PW, McGeachie JM, Davies MJ, Grounds MD. Evans Blue Dye as an *in vivo* marker of myofibre damage: optimising parameters for detecting initial myofibre membrane permeability. J Anat 2002;200(Pt 1):69–79. https://doi.org/10.1046/j.0021-8782.2001.00008.x. PubMed PMID: 11837252; PubMed Central PMCID: PMCPMC1570883.

[16] Sessegolo C, Cruaud C, Da Silva C, Cologne A, Dubarry M, Derrien T, et al. Transcriptome profiling of mouse samples using nanopore sequencing of cDNA and RNA molecules. Sci Rep 2019;9(1):14908. https://doi.org/10.1038/s41598-019-51470-9.

[17] Rosenthal SM. IGFs and Skeletal Muscle. In: Rosenfeld RG, Roberts CT, editors. The igf system: molecular biology, physiology, and clinical applications. Totowa, NJ: Humana Press; 1999. p. 497–516.

[18] Barton ER, Morris L, Musaro A, Rosenthal N, Sweeney HL. Muscle-specific expression of insulin-like growth factor I counters muscle decline in mdx mice. J Cell Biol 2002;157(1):137–48. https://doi.org/10.1083/jcb.200108071. Epub 2002/04/03PubMed PMID: 11927606; PubMed Central PMCID: PMCPMC2173262.

[19] Shavlakadze T, White J, Hoh JF, Rosenthal N, Grounds MD. Targeted expression of insulin-like growth factor-I reduces early myofiber necrosis in dystrophic mdx mice. Mol Ther 2004;10(5):829–43. https://doi.org/10.1016/j.ymthe.2004.07.026. Epub 2004/10/29PubMed PMID: 15509501.

[20] Schertzer JD, Ryall JG, Lynch GS. Systemic administration of IGF-I enhances oxidative status and reduces contraction-induced injury in skeletal muscles of mdx dystrophic mice. Am J Physiol Endocrinol Metab 2006;291(3):E499–505. https://doi.org/10.1152/ajpendo.00101.2006. Epub 2006/04/20PubMed PMID: 16621899.

[21] Gregorevic P, Plant DR, Leeding KS, Bach LA, Lynch GS. Improved contractile function of the mdx dystrophic mouse diaphragm muscle after insulin-like growth factor-I administration. Am J Pathol 2002;161(6):2263–72. https://doi.org/10.1016/s0002-9440(10)64502-6. Epub 2002/12/06PubMed PMID: 12466140; PubMed Central PMCID: PMCPMC1850914.

[22] Allard JB, Duan C. IGF-binding proteins: why do they exist and why are there so many? Front Endocrinol (Lausanne) 2018;9:117. https://doi.org/10.3389/fendo.2018.00117. Epub 2018/04/25PubMed PMID: 29686648; PubMed Central PMCID: PMCPMC5900387.

[23] Rodrigues M, Echigoya Y, Maruyama R, Lim KR, Fukada SI, Yokota T. Impaired regenerative capacity and lower revertant fibre expansion in dystrophin-deficient

mdx muscles on DBA/2 background. Sci Rep 2016;6:38371. https://doi.org/10.1038/srep38371. Epub 2016/12/08PubMed PMID: 27924830; PubMed Central PMCID: PMCPMC5141435.
[24] Yoshida T, Delafontaine P. Mechanisms of IGF-1-mediated regulation of skeletal muscle hypertrophy and atrophy. Cells 2020;9(9). https://doi.org/10.3390/cells9091970. Epub 2020/08/30PubMed PMID: 32858949; PubMed Central PMCID: PMCPMC7564605.
[25] Marchalot A, Horiot C, Lambert J-M, Carrion C, Oblet C, Pollet J, et al. Targeting IgE polyadenylation signal with antisense oligonucleotides decreases IgE secretion and plasma cell viability. J Allergy Clin Immunol 2022;149(5):1795–801. https://doi.org/10.1016/j.jaci.2021.09.039.
[26] Marsollier AC, Joubert R, Mariot V, Dumonceaux J. Targeting the polyadenylation signal of Pre-mRNA: a new gene silencing approach for facioscapulohumeral dystrophy. Int J Mol Sci 2018;19(5). https://doi.org/10.3390/ijms19051347. Epub 2018/05/13PubMed PMID: 29751519; PubMed Central PMCID: PMCPMC5983732.
[27] Vickers TA, Wyatt JR, Burckin T, Bennett CF, Freier SM. Fully modified 2′ MOE oligonucleotides redirect polyadenylation. Nucleic Acids Res 2001;29(6):1293–9. https://doi.org/10.1093/nar/29.6.1293. Epub 2001/03/10PubMed PMID: 11238995; PubMed Central PMCID: PMCPMC29745.
[28] Spangenburg EE, Abraha T, Childs TE, Pattison JS, Booth FW. Skeletal muscle IGF-binding protein-3 and -5 expressions are age, muscle, and load dependent. Am J Physiol Endocrinol Metab 2003;284(2):E340–50. https://doi.org/10.1152/ajpendo.00253.2002. Epub 2002/10/25PubMed PMID: 12397024.
[29] Barclay RD, Burd NA, Tyler C, Tillin NA, Mackenzie RW. The role of the IGF-1 signaling cascade in muscle protein synthesis and anabolic resistance in aging skeletal muscle. Front Nutr 2019;6:146. https://doi.org/10.3389/fnut.2019.00146. Epub 20190910PubMed PMID: 31552262; PubMed Central PMCID: PMCPMC6746962.
[30] Rotwein P. Diversification of the insulin-like growth factor 1 gene in mammals. PLoS One 2017;12(12):e0189642. https://doi.org/10.1371/journal.pone.0189642. Epub 20171214PubMed PMID: 29240807; PubMed Central PMCID: PMCPMC5730178.
[31] Curinha A, Oliveira Braz S, Pereira-Castro I, Cruz A, Moreira A. Implications of polyadenylation in health and disease. Nucleus 2014;5(6):508–19. https://doi.org/10.4161/nucl.36360. Epub 20141031PubMed PMID: 25484187; PubMed Central PMCID: PMCPMC4615197.